Therapeutic efficacy of an oral nucleoside analog of remdesivir against SARS-CoV-2 pathogenesis in mice.

Alexandra Schäfer [1, 4], David R. Martinez [1, 4], John J. Won [1], Fernando R. Moreira [1], Ariane J. Brown [1], Kendra L. Gully [1], Rao Kalla [2], Kwon Chun [2], Venice Du Pont [2], Darius Babusis [2], Jennifer Tang [2], Eisuke Murakami [2], Raju Subramanian [2], Kimberly T Barrett [2], Blake J. Bleier [2], Roy Bannister [2], Joy Y. Feng [2], John P. Bilello [2], Tomas Cihlar [2], Richard L. Mackman [2], Stephanie A. Montgomery [3], Ralph S. Baric [1], Timothy P. Sheahan [1, *]

[1] Department of Epidemiology, University of North Carolina at Chapel Hill, Chapel Hill, NC, USA,

[2] Gilead Sciences, Inc, Foster City, CA, USA,

[3] Department of Pathology and Laboratory Medicine, University of North Carolina School of Medicine, Chapel Hill, NC, USA,

[4] These authors contributed equally to this manuscript.

[*] Timothy P. Sheahan. sheahan@email.unc.edu

Abstract

The COVID-19 pandemic remains uncontrolled despite the rapid rollout of safe and effective SARS-CoV-2 vaccines, underscoring the need to develop highly effective antivirals. In the setting of waning immunity from infection and vaccination, breakthrough infections are becoming increasingly common and treatment options remain limited. Additionally, the emergence of SARS-CoV-2 variants of concern with their potential to escape therapeutic monoclonal antibodies emphasizes the need to develop second-generation oral antivirals targeting highly conserved viral proteins that can be rapidly deployed to outpatients. Here, we demonstrate the in vitro antiviral activity and in vivo therapeutic efficacy of GS-621763, an orally bioavailable prodrug of GS-441524, the parental nucleoside of remdesivir, which targets the highly conserved RNA-dependent RNA polymerase. GS-621763 exhibited significant antiviral activity in lung cell lines and two different human primary lung cell culture systems.

35 The dose-proportional pharmacokinetic profile observed after oral administration of GS-621763
36 translated to dose-dependent antiviral activity in mice infected with SARS-CoV-2. Therapeutic
37 GS-621763 significantly reduced viral load, lung pathology, and improved pulmonary function
38 in COVID-19 mouse model. A direct comparison of GS-621763 with molnupiravir, an oral
39 nucleoside analog antiviral currently in human clinical trial, proved both drugs to be similarly
40 efficacious. These data demonstrate that therapy with oral prodrugs of remdesivir can
41 significantly improve outcomes in SARS-CoV-2 infected mice. Thus, GS-621763 supports the
42 exploration of GS-441524 oral prodrugs for the treatment of COVID-19 in humans.
43

44 **Introduction**

45 SARS-CoV-2 emerged in December 2019 and has caused 223 million infections and 4.6
46 million deaths worldwide as of September 2021 (*1-3*). While there are multiple effective
47 vaccines, vaccination rates have lagged in the United States (U.S.) due to vaccine hesitancy and
48 public mistrust thus delaying the generation of herd immunity required to significantly diminish
49 community spread. In addition, outside of the U.S., many countries do not have equitable access
50 to vaccines and/or have been slow to vaccinate (*4-7*). This collective constellation of events is
51 fueling the generation of viral variants that are increasingly transmissible and are ever evolving
52 to escape human immunity. Therefore, there is an immediate unmet need for oral antivirals that
53 can be rapidly disseminated to treat COVID-19 cases in the unvaccinated, the
54 immunocompromised and in vaccine breakthrough cases. Next-generation oral coronavirus
55 (CoV) antivirals, if widely disseminated and given early in infection, could curtail the duration of
56 disease, reduce long-term sequelae of COVID-19, minimize household transmissions, and lessen
57 hospitalizations, thus having a broad impact on public health.

58 There are multiple direct-acting antiviral (DAA) therapies in use to treat COVID-19 (*8-*
59 *12*), including Emergency Use Authorization (EUA)-approved monoclonal antibodies (mAbs)
60 and FDA-approved remdesivir (RDV, GS-5734). Monoclonal antibodies have demonstrated
61 efficacy for treating active COVID-19 cases in outpatients (Regeneron outpatient studies) but
62 currently, all mAbs must be administered via injection, limiting their use to those with ready
63 access to healthcare (*13, 14*). In addition, several SARS-CoV-2 variants of concern (VOCs) have
64 evolved that are resistant to first-line mAb therapies (*15, 16*). Currently, RDV is the only FDA-
65 approved small-molecule direct-acting antiviral to treat COVID-19, but there are several other
66 DAAs currently in human clinical trials including nucleoside analogs molnupiravir (MPV,
67 EIDD-2801) and AT-527, as well as MPro inhibitor PF-07321332 (*17-25*) . Unlike mAbs which
68 specifically target the virion surface exposed spike protein of SARS-CoV-2, nucleoside analog
69 drugs target a highly conserved viral enzyme among CoV, the RNA-dependent RNA polymerase
70 (RdRp) nsp12, rendering them broadly active against multiple emerging, endemic and enzootic
71 CoV. Moreover, due to its high degree of conservation among CoV, the RdRp likely does not
72 have the same capacity for mutational change as spike, which may translate into RdRp having a
73 higher barrier to resistance (*18-20*). Despite demonstrated therapeutic efficacy of RDV against
74 SARS-CoV-2 in animal models (*17, 23, 26*) and in human clinical trials (*8*), the requirement of
75 intravenous administration has limited its widespread use during this pandemic. The orally
76 bioavailable nucleoside prodrug GS-621763, is designed for optimal delivery of the parent
77 nucleoside GS-441524 into systemic circulation, which is then metabolized inside cells into the
78 same active nucleoside triphosphate formed by RDV (*27*). Here, we detail the *in vitro* antiviral
79 activity in various cell models and *in vivo* therapeutic efficacy of oral GS-621763 in a mouse
80 model of SARS-CoV-2 pathogenesis.

81

82 **Results**

83 **GS-621763 has antiviral activity against SARS-CoV-2 in cell lines and human primary cell**
84 **cultures.**

85 GS-441524 is the parental adenosine nucleoside analog (Fig. 1A) of both
86 monophosphoramidate prodrug RDV (GS-5734, Fig. 1B), and triester prodrug GS-621763 (Fig.
87 1C). All three molecules are metabolized to the same active nucleotide triphosphate in cells, but
88 through different activation pathways. GS-621763 is rapidly metabolized during oral absorption
89 to GS-441524, then intracellularly converted by cellular kinases to the analog monophosphate
90 metabolite before further metabolism to the active nucleoside triphosphate. In contrast, the intact
91 phosphoramidate prodrug, RDV, is broken down inside cells directly to the same monophosphate
92 metabolite, effectively bypassing the rate-limiting first phosphorylation step of GS-441524 (*27*).
93 To determine if GS-621763 could inhibit replication of SARS-CoV-2 in cellular assays, we first
94 evaluated its antiviral activity against a SARS-CoV-2 reporter virus expressing nanoluciferase
95 (SARS-CoV-2 nLUC) in A549-hACE2 cells stably expressing the human entry receptor
96 angiotensin-converting enzyme 2 (ACE2) (*28*). With GS-621763, we observed a dose-dependent
97 antiviral effect on SARS-CoV-2 nLUC replication with an average half-maximum effective
98 concentration (EC_{50}) of 2.8 μM (Fig. 1D, Fig.1H, and Supplementary Figure 1A). In the same
99 assay, we measured EC_{50} values for the control compound RDV of 0.28 μM, similar to those
100 reported previously in these cells and reflective of the enhanced ability of the phosphoramidate
101 prodrug to rapidly and efficiently generate active triphosphate by bypassing the slower initial
102 phosphorylation step (Fig. 1D, Fig. 1H, Supplementary Figure 1A) (*29*). As was observed in
103 other cell systems, the parental nucleoside, GS-441524, was less potent (EC_{50} = 3.3 μM) than

104 RDV in our assay and was similar in potency to GS-621763. This suggests that the tri-isobutyryl
105 esters of GS-621763 are efficiently cleaved in the assay to release GS-441524 (Fig. 1D, Fig. 1H,
106 Supplementary Figure 1A). Importantly, we did not observe any measurable cytotoxicity of any
107 of the inhibitors in A549-hACE2 cells at concentrations up to 10 μM (Figure 1F, Supplementary
108 Figure 1B). Human primary airway epithelial (HAE) cell cultures model the cellular complexity
109 and architecture of the human conducting airway and are often used to determine if drugs are
110 transported and metabolized in the cells targeted by emerging CoV in vivo (*18*). In HAE cells
111 infected with WT SARS-CoV-2 (*28*) and treated with GS-621763, we observed a dose-
112 dependent and significant reduction in infectious virus production as compared to DMSO-
113 vehicle treated cultures (Fig. 1F). In similarly infected, control compound (i.e. RDV or GS-
114 441524) treated cultures, a significant and dose-dependent reduction in viral titers was also
115 observed (Fig. 1F). GS-621763, RDV, and GS-441524 inhibited reporter SARS-CoV-2
116 expressing Firefly luciferase (SARS-CoV-2 Fluc) replication in normal human bronchial
117 epithelial (NHBE) cultures with EC_{50} values of 0.125, 0.0371, and 2.454 μM, respectively (Fig.
118 1G, Fig. 1H). All together, these data show that GS-621763 is transported, metabolized and
119 potently antiviral human primary cell systems that model the tissues targeted by SARS-CoV-2 in
120 humans.
121
122 **Dose-dependent therapeutic efficacy of GS-621763 in mouse models of COVID-19 disease.**
123 We have previously performed multiple studies describing the therapeutic efficacy of
124 subcutaneously administered RDV in mice (*Ces1c*$^{-/-}$ C57BL/6J) genetically deleted for a secreted
125 plasma carboxylesterase 1c (*Ces1c*) absent in humans but dramatically reduces drug half-life in
126 wild-type mice (*17-19, 26, 30*).

127 However, the prodrug GS-621763 is designed to be rapidly cleaved pre-systemically in
128 vivo to release GS-441524 into circulation, with no or very minimal intact ester observed in
129 plasma. Therefore, GS-621763 can be studied in wild-type mice where it should also be rapidly
130 converted to parent GS-441524. Plasma pharmacokinetics following a single oral administration
131 of GS-621763 at either 5 or 20 mg/kg were first determined in uninfected BALB/c mice (Fig.
132 2A). Doses were selected to provide high plasma exposures of GS-441524 that would support
133 active triphosphate formation in the lung and to confirm pharmacokinetic dose proportionality
134 needed to project exposures in efficacy studies. Previous studies had shown that parent
135 nucleoside was at least 10-fold less efficient at generating lung triphosphate than RDV, on a
136 molar basis, thus requiring higher plasma exposures of parental GS-441524 to account for the
137 reduced metabolic efficiency (*27*). No exposure of intact ester prodrug, within the limit of
138 detection, was observed in mice. GS-441524 was both rapidly absorbed and then cleared from
139 systemic circulation, exhibiting a short plasma half-life of approximately 1 hr. Dose
140 proportional increases in both maximal plasma concentrations (C_{max}) and exposures ($AUC_{0\text{-}24h}$)
141 at the two doses were observed (Fig. 2A).

142 To better understand the pharmacokinetic and pharmacodynamic relationship for GS-
143 621763, we performed a series of dose-finding studies in BALB/c mice infected with mouse-
144 adapted SARS-CoV-2 (SARS-CoV-2 MA10) (*30*). In young adult BALB/c mice infected with
145 10^4 plaque forming units (PFU) SARS-CoV-2 MA10, virus replicates to high titers in the
146 respiratory tract, mice lose 15-20% of their body weight by 4 days post-infection (dpi), and acute
147 lung injury/loss of pulmonary function is typically observed after virus replication peaks on 2 dpi
148 (*30*). We first defined the minimum dosage sufficient for maximal therapeutic efficacy in
149 BALB/c mice initiating twice daily (i.e. bis in die, BID) oral treatment with either vehicle control

150 or 3 mg/kg, 10 mg/kg, or 30 mg/kg GS-621763 beginning 8 hours post infection (hpi) with 10^4
151 PFU SARS-CoV-2 MA10 (Fig. 2B). Unlike vehicle or 3 mg/kg GS-621763 treated animals,
152 mice receiving either 10 or 30 mg/kg GS-621763 were completely protected from weight loss
153 thus demonstrating that early oral antiviral therapy can prevent the progression of disease (Fig.
154 2B). Congruent with the weight loss phenotype, both 10 and 30 mg/kg GS-621763 treated
155 animals had significantly reduced viral lung titers as compared to both the vehicle and 3 mg/kg
156 treated groups (Fig. 2C). To monitor the effect of drug treatment on pulmonary function, we
157 performed daily whole-body plethysmography (WBP) with a subset of mice from each group
158 (N=4 per treatment group). As shown with the WBP metric PenH, whose elevation is associated
159 with airway resistance or obstruction (*18*), we observed a drug dose-dependent reduction in
160 PenH with the maximal effect seen in the 30 mg/kg GS-621763 dose group which was
161 completely protected from the loss of pulmonary function observed in the other treatment groups
162 and vehicle (Fig. 2D). Mice treated with 3 and 10 mg/kg GS-621763 had impaired lung function
163 at days 2 and 3 post infection, but lung function returned to baseline by 4 dpi for all GS-621763
164 treated animals (Fig. 2D). Consistent with weight loss, virus titer, and pulmonary function data,
165 mice treated with 10 or 30 mg/kg had significantly reduced lung congestion, a gross pathologic
166 feature characteristic of severe lung damage (Fig. 2E). We then scored lung tissue sections for
167 the histologic features of acute lung injury (ALI) using two complementary semiquantitative
168 tools. First, using an ALI scoring tool created by the American Thoracic Society (ATS), we
169 blindly evaluated three diseased fields per lung section for several features of ALI including
170 alveolar septal thickening, neutrophils in the interstitium and in air spaces, proteinaceous debris
171 in airspaces, and the presence of hyaline membranes. Only mice treated with 30 mg/kg had
172 significantly reduced ALI scores (Fig. 2F). Second, we used a complementary tool measuring

173 the pathologic hallmark of ALI, diffuse alveolar damage (DAD). Mice in all treated groups
174 showed reduced DAD scores, but only mice receiving 30 mg/kg had significantly decreased
175 DAD in their lungs (Fig. 2G). Together, these data demonstrate that the oral delivery of the
176 nucleoside analog GS-621763 can significantly diminish SARS-CoV-2 virus replication and
177 associated pulmonary disease in a dose-dependent manner.
178

179 **Extended therapeutic protection against COVID-19 disease by GS-621763 in mice**

180 To determine if the potent therapeutic efficacy of GS-621763 observed with early
181 intervention (8 hr after infection) would extend to later times post infection, we designed a
182 therapeutic efficacy study with six arms where we varied both time of oral therapy initiation and
183 dose level in BALB/c mice infected with SARS-CoV-2 MA10 (Fig.3). As done previously, a
184 control group of animals received vehicle twice daily beginning at 12 hours post infection (hpi).
185 The next three arms of the study were dedicated to the 30 mg/kg GS-621763 dose level, with two
186 of the three arms receiving twice daily dosing initiated at either the 12 hpi ("30 mg/kg BID 12
187 hr" group) or the 24 hpi ("30 mg/kg BID 24 hr" group). The third 30 mg/kg arm was designed to
188 determine if dose frequency could be reduced to once daily (quaque die, QD) if initiated early at
189 12 hpi ("30 mg/kg QD 12 hr" group). In the last two arms, we wanted to evaluate if an increased
190 dose of 60 mg/kg given QD beginning at 12 hr or 24 hr ("60 mg/kg QD 12 hr" and "60 mg/kg
191 QD 24 hr" groups) would improve outcomes over the 30 mg/kg groups. Initiation of 30 mg/kg
192 BID therapy at either 12 or 24 hrs offered significant protection from weight loss (Fig. 3A),
193 extending the robust therapeutic phenotype observed for this dose level when initiated at very
194 early times (at 8 hr) (Fig 2). Interestingly, when we decreased the frequency of 30 mg/kg
195 treatment initiated at 12 hr to once daily ("30 mg/kg QD 12 hr" group), we also observed a

196 significant prevention of body weight loss (Fig 3A), thus levels of drug when administered once
197 a day and begun early (at 12 hr) in the course of infection were sufficient to prevent disease
198 progression. Increasing the dose to 60 mg/kg QD initiated at either 12 hr or 24 hr offered similar
199 protection from weight loss observed with vehicle treatment as the 30 mg/kg groups (Fig. 3A).
200 As body weight loss is a crude marker of viral pathogenesis, we next measured multiple
201 virological, physiologic, and pathologic metrics of disease. First, we measured the levels of
202 infectious virus present in lung tissue on 4 dpi. Unlike vehicle-treated animals who harbored an
203 average titer of $5.6x10^4$ PFU per lung lobe, all GS-621763 dose groups significantly reduced the
204 levels of infectious virus in lung tissue with the average titers of most groups falling below the
205 limit of detection (90 PFU). Interestingly, 30 mg/kg delivered QD had significantly elevated
206 viral lung titers (mean titer = $4x10^2$ PFU) as compared to its BID counterpart (mean titer = < 90
207 PFU). A similar trend among treatment groups was observed when measuring the levels of
208 SARS-CoV-2 subgenomic and genomic nucleocapsid (N) RNA in parallel lung tissues (Fig. 3C).
209 All 30 mg/kg groups significantly reduced levels of SARS-CoV-2 RNA in lung tissue as
210 compared to vehicle-treated animals. As observed for infectious titers, 30 mg/kg given QD daily
211 beginning at 12 hr had elevated levels of N RNA as compared to 30 mg/kg given BID beginning
212 at 12 hr suggesting that trough and/or daily exposure levels of drug with QD dosing are
213 insufficient to suppress replication similarly to BID dosing. Increasing the once-daily dose to 60
214 mg/kg to raise the daily exposure and trough levels offered similar reductions in SARS-CoV-2 N
215 RNA as compared to 30 mg/kg BID when initiated at 12 hr, but the levels of viral RNA in the
216 higher dose 60mg/kg group initiated at 24 hr were not different than vehicle (Fig. 3C). Although
217 vehicle-treated animals exhibited significant loss of pulmonary function as measured by WBP,
218 this was largely prevented with GS-621763 therapy (Fig. 3D). All therapy groups initiated at 12

219 hr were equally protected from loss of pulmonary function as measured by the PenH metric (Fig.
220 3D). Of all groups actively receiving GS-621763, animals in the 30 mg/kg BID 24 hr group had
221 a measurable loss of lung function on 3 dpi which resolved by 4 dpi but this phenotype was not
222 extended to other groups. We then scored lung tissue sections for the histologic features of acute
223 lung injury and alveolar damage. Only 30 mg/kg BID initiated at 12 hr significantly reduced ALI
224 scores as compared to those in vehicle-treated animals. In addition, the 30 mg/kg BID 12 hr-
225 group had significantly lower ALI scores as compared to the 60 mg/kg QD 24 hr-group (Figure
226 3E). Only 30 mg/kg given twice a day at 12 hr most dramatically reduced DAD scores but this
227 protection from lung pathology was lost if given once per day or if initiated at 24 hr (Fig. 3G).
228 The high dose of 60 mg/kg QD when initiated at 12 hr improved DAD scores as compared to
229 similarly treated animals that began treatment at 24 hr. Collectively, these data demonstrate that
230 GS-621763 therapy can improve both virologic and pathogenic metrics, but the degree of
231 improvement was dependent on time of initiation and dose frequency.
232

233 **The therapeutic efficacy of GS-621763 is similar to molnupiravir (MPV, EIDD-2801)**

234 MPV is an oral nucleoside analog prodrug antiviral currently in Phase 3 clinical trial to
235 treat COVID-19 with demonstrated antiviral efficacy in mice against several emerging CoV
236 including SARS-CoV, MERS-CoV, and SARS-CoV-2 (*18, 19, 21, 22*). Like GS-621763, MPV
237 is a prodrug which is metabolized in vivo into a parental nucleoside (β-D-N4-hydroxycytidine,
238 NHC) in its metabolic progression towards the antiviral active triphosphate (*20*). To determine if
239 GS-621763 would provide similar protection as MPV, we then designed comparative therapeutic
240 efficacy studies in the mouse model of SARS-CoV-2 pathogenesis described above. Pre-efficacy
241 pharmacokinetic studies in BALB/c mice (30 mg/kg or 100 mg/kg) were performed with MPV

242 and showed dose proportional increases in NHC plasma exposures (Supplemental Fig. 2).
243 Pharmacokinetic modeling then determined that a daily 120 mg/kg dose (given 60 mg/kg BID)
244 would result in exposures similar to that observed in humans receiving 800 mg BID, a dose
245 being evaluated in a human clinical trial (*22*). The comparative efficacy study included a vehicle
246 group and 5 additional groups receiving two doses of MPV or GS-621763 per day 12 hrs apart
247 (BID). Three arms of the study began dosing at 12 hr: 30 mg/kg GS-621763, 30 mg/kg MPV
248 (0.5× human equivalent dose) or 60 mg/kg MPV (1× human equivalent dose). At 24 hr, we
249 began dosing of two additional groups: 60 mg/kg GS-621763 or 60 mg/kg MPV. While SARS-
250 CoV-2 MA10 infection caused rapid weight loss in vehicle control animals, all animals receiving
251 either GS-621763 or MPV beginning at either 12 or 24 hr were protected from weight loss (Fig.
252 4A). Similarly, upon titration of lung tissues at 4 dpi for infectious virus by plaque assay,
253 vehicle-treated animals had expectedly high levels of infectious virus which was significantly
254 reduced in all treatment groups, independent of drug type or initiation time (Fig. 4B). When
255 treatment was initiated at 12 hr, a moderate yet significant elevation in infectious titers was
256 observed in the 30mg/kg MPV group, inferior to either equivalently dosed GS-621763 animals
257 or those receiving the higher dose (60 mg/kg) of MPV (Fig. 4B). To understand the relationship
258 between levels of infectious virus and viral RNA in lung tissue, we performed qRT-PCR on total
259 RNA for SARS-CoV2 N RNA in parallel tissues utilized for plaque assay. The trend observed
260 with infectious virus is mirrored in the qRT-PCR data where all groups receiving antiviral
261 therapy had significantly reduced levels of viral RNA (Fig. 4C). In addition, animals receiving
262 30 mg/kg MPV (0.5× human equivalent dose) had a measurable increase in N RNA as compared
263 to equivalently dosed GS-621763 animals. Similar to weight loss data, vehicle-treated animals
264 had a significant loss of pulmonary function as measured by WBP on both 3 and 4 dpi which was

265 prevented in all groups receiving antiviral treatment (Fig. 4D). We then blindly evaluated lung
266 tissue sections for the pathological manifestations of ALI and DAD using two complementary
267 histologic tools described above. Congruent with the above data, ALI scores in all antiviral
268 therapy groups were significantly reduced as compared to vehicle controls (Fig. 4E). In
269 agreement with ALI scores, the DAD histologic scores were similarly reduced in all antiviral
270 therapy treated groups as compared to those treated with vehicle (Fig. 4F). All together, these
271 data show that antiviral therapy with GS-621763 and MPV when initiated early or at the peak of
272 virus replication (~24 hr) can both significantly diminish virus replication and improve disease
273 outcomes.
274

275 **Discussion**

276 Three novel human CoVs have emerged in the past 20 years, first with SARS-CoV in
277 2002-2003, MERS-CoV in 2012 and most recently, SARS-CoV-2 in 2019 (*1, 2, 31*). Vaccine
278 availability, vaccine hesitancy, and the ongoing evolution and emergence of VOCs are
279 collectively delaying the global control of pandemics and potential achievement of global herd
280 immunity and may prevent it altogether (*15, 32-34*). As such, there is an acute need for broad-
281 spectrum antivirals to treat COVID-19 in the unvaccinated as well as increasingly common
282 breakthrough infections in those vaccinated, driven by immune evading VOCs. In addition, due
283 to the emergence potential of the CoV family, we must also actively develop broadly acting
284 therapies effective the CoVs of today to prepare for those that may emerge in the future. Both
285 RDV and MPV are examples of nucleoside analogs with broad activity against genetically
286 diverse CoV (*35*). Here, we show that GS-621763, a prodrug that improves the oral delivery of

287 parent nucleoside GS-441524, is yet another example of an orally bioavailable nucleoside analog
288 prodrug that is effective against SARS-CoV-2.

289 Oral broadly acting antiviral therapies that target conserved viral proteins with a
290 diminished capacity for evolutionary change will maximize therapeutic utility against future
291 emerging CoV. SARS-CoV-2 has undergone a considerable amount of genetic evolution since
292 its emergence in 2019; each time a globally dominant SARS-CoV-2 VOC has emerged, it has
293 been replaced by a new VOC harboring more concerning characteristics like replicative capacity
294 or transmissibility (*36*). The majority of genetic changes have been localized to viral proteins
295 decorating the surface of the virus particle like the viral spike which has mutated to eradicate
296 epitopes targeted by early and promising monoclonal antiviral therapies (e.g. Eli Lily,
297 Regeneron) rendering them less active against newer VOCs (*37*). Approved antivirals like RDV,
298 those in clinical trials like MPV, AT-527, and PF-07321332 (Pfizer, oral protease inhibitor)
299 target highly conserved enzymes required for virus replication which likely have a diminished
300 capacity for change as compared to the spike protein (*38*). The widespread use of both RDV and
301 mAb therapies in the U.S. and globally has been limited by the necessity of delivery by
302 intravenous infusion which in turn requires access to qualified health care staff and facilities.
303 Thus, effective oral antiviral therapy or combination therapies which can be procured at a
304 pharmacy and self-administered by the patient would help facilitate wide-spread global access
305 and could have profound positive impacts on global public health.

306 In this study, we utilized a mouse adapted SARS-CoV-2 variant, SARS-CoV-2 MA10, in
307 wild-type BALB/c mice. (*17, 30*). Mice infected with this virus develop severe lung disease
308 reminiscent of that seen with severe COVID-19 including the development of ALI and
309 respiratory failure (*30*). It is important to note that the disease resulting from SARS-CoV-2

310 MA10 infection in mice is compressed as compared to that observed in humans with virus titer
311 peaking in the mouse lung between 24-48 hrs after infection, rapid loss of pulmonary function
312 beginning 2-3 dpi, rapid weight loss within the first 4 days of infection, lung pathology
313 consistent with ALI peaking 4-6 dpi and virus induced mortality within a week of infection. This
314 is markedly different than the COVID-19 in humans where virus titers peak in the upper airway
315 within the first week, but viral RNA shedding can be observed for as long as 24 days and
316 symptoms can take weeks to months to resolve (*39-41*). Because of this caveat associated with
317 our mouse model, the time in which to intervene with a direct acting antiviral and sufficiently
318 improve outcomes is curtailed in mice as compared to humans. Our recent study with RDV
319 exemplifies this where we found the degree of therapeutic benefit in mice infected with SARS-
320 CoV-2 MA10 was dependent on the time of initiation (*17*). Here, we show that oral
321 administration with GS-621763 prevents body weight loss, loss of pulmonary function, severe
322 lung pathology and virus replication when administered at 12 and 24 hrs after infection. While
323 we observed improvement in some metrics with RDV initiated at 24 hr in our prior studies (*17*),
324 GS-621763 therapy initiated at a similar time comparatively improved all metrics assessed.
325 Thus, herein we provide proof-of-concept preclinical data that the orally bioavailable ester
326 analog of RDV GS-621763 can exert potent antiviral effects in vivo during an ongoing SARS-
327 CoV-2 infection. Lastly, we show that GS-621763 therapy provides similar levels of protection
328 from SARS-CoV-2 pathogenesis as MPV, an oral nucleoside analog prodrug effective against
329 SARS-CoV-2 in mice that is currently in human clinical trials. Future directions are focused on
330 extending these studies to evaluate the efficacy of combinations of antivirals in our models of
331 SARS-CoV-2 pathogenesis and in other models that can evaluate the blockade of transmission
332 such as hamster and ferret.

333 In summary, we provide preclinical data demonstrating the in vitro antiviral activity and
334 in vivo therapeutic efficacy of an orally bioavailable nucleoside analog prodrug, GS-621763. The
335 data provided herein supports the future evaluation of orally bioavailable prodrugs of GS-441524
336 in humans with COVID-19. If safe and effective, this class of RdRp inhibitors could become part
337 of the arsenal of existing oral antivirals that are desperately needed to address a global unmet
338 need for the COVID-19 pandemic and CoV pandemics of the future.
339

340 **Figure Legends**

341 **Figure 1. Chemical Structure and in vitro potency of GS-621763 in comparison to RDV**
342 **(GS-5734) and GS-441524.**

343 (A) Chemical structure of the parental adenosine nucleoside analog GS-441524.
344 (B) Chemical structure of the monophosphoramidate prodrug RDV.
345 (C) Chemical structure of GS-621763, the tri-isobutyryl ester of GS-441524.
346 (D) Mean percent inhibition of SARS-CoV-2 replication by GS-621763, in comparison to the
347 prodrug RDV - and the parental nucleoside GS-441524 in A459-hACE2 cells (done in
348 triplicates).
349 (E) Cytotoxicity in A459-hACE2 cells treated with GS-621763, RDV, and GS-441524 in A459-
350 hACE2 cells (done in triplicates, CellTiter-Glo – CTG).
351 (F) Inhibition of SARS-CoV-2 replication by GS-621763, in comparison to the prodrug RDV
352 and the parental nucleoside GS-441524 in human primary airway epithelial cells (HAE, done in
353 duplicates).

354 (G) Inhibition of SARS-CoV-2-Fluc replication by GS-621763, RDV -, and the parental
355 nucleoside GS-441524 in normal human bronchial epithelial (NHBE) cultures (done in
356 duplicates).
357 (H) In vitro EC_{50} values for inhibition of viral replication by GS-621763, RDV, and the parental
358 nucleoside GS-441524 in A459-hACE2 and NHBE cells.
359
360 **Figure 2. Dose-dependent therapeutic protection against COVID-19 disease by GS-621763**
361 **in mice.**
362 (A) Plasma Pharmacokinetics of GS-441524 in uninfected Balb/c mice following a single oral
363 administration of GS-621763 at either 5 or 20 mg/kg. Plasma concentrations of GS-621763 were
364 below the limit of quantification at all time points.
365 (B) Depicted is the % starting weight in therapeutically treated mice with vehicle (n=19) or 3
366 mg/kg (n=9), 10 mg/kg (n=10), and 30 mg/kg (n=10) GS-621763 at 8 hr. All mice were infected
367 with $1x10^4$ PFU SARS-CoV-2 MA10.
368 (C) Lung viral titers in therapeutically treated mice with vehicle (n=19) or 3 mg/kg (n=9), 10
369 mg/kg (n=10), and 30 mg/kg (n=10) GS-621763 at 8 hr. All mice were infected with $1x10^4$ PFU
370 SARS-CoV-2 MA10. Limit of detection (LoD)
371 (D) Pulmonary function in therapeutically treated mice with vehicle (n=4) or 3 mg/kg (n=4), 10
372 mg/kg (n=4), and 30 mg/kg (n=4) GS-621763 at 8 hr. All mice were infected with $1x10^4$ PFU
373 SARS-CoV-2 MA10.
374 (E) Lung congestion score in therapeutically treated mice with vehicle (n=19) or 3 mg/kg (n=9),
375 10 mg/kg (n=10), and 30 mg/kg (n=10) GS-621763 at 8 hr. All mice were infected with $1x10^4$
376 PFU SARS-CoV-2 MA10.

377 (F and G) Lung pathology in the therapeutically treated mice with vehicle (n=19) or 3 mg/kg
378 (n=9), 10 mg/kg (n=10), and 30 mg/kg (n=10) GS-621763 at 8 hr. All mice were infected with
379 $1x10^4$ PFU SARS-CoV-2 MA10.
380 Data were analyzed using two-way ANOVA (weight loss and lung function) and Kruskal-Wallis
381 test (lung titer, congestion score, and pathology scores), *p<0.05, **p<0.005, ***p<0.0005,
382 ****p<0.0001
383
384 **Figure 3. Extended therapeutic protection of mice against COVID-19 disease by oral GS-**
385 **621763 in mice.**
386 (A) Depicted is the % starting weight in therapeutically treated mice with either 30 mg/kg or 60
387 mg/kg BID or QD GS-621763 at 12 and 24 hrs (n=10 for all treatment groups, except n=8 for 60
388 mg/kg, 12 hr QD treatment group). All mice were infected with $1x10^4$ PFU SARS-CoV-2
389 MA10.
390 (B) Lung viral titers in therapeutically treated mice with either 30 mg/kg or 60 mg/kg BID or QD
391 GS-621763 at 12 and 24hrs (n=10 for all treatment groups, except n=8 for 60 mg/kg, 12 hr QD
392 treatment group). All mice were infected with $1x10^4$ PFU SARS-CoV-2 MA10. Limit of
393 detection (LoD).
394 (C) Viral N RNA in therapeutically treated mice with either 30 mg/kg or 60 mg/kg BID or QD
395 GS-621763 at 12 and 24 hrs (n=10 for all treatment groups, except n=8 for 60 mg/kg, 12 hr QD
396 treatment group). All mice were infected with $1x10^4$ PFU SARS-CoV-2 MA10.
397 (D) Pulmonary function in therapeutically treated mice with either 30 mg/kg or 60 mg/kg BID or
398 QD GS-621763 at 12 and 24 hrs (n=4 for all treatment groups). All mice were infected with
399 $1x10^4$ PFU SARS-CoV-2 MA10.

400 (n=4 for all treatment groups).

401 (F and G) Lung pathology in the therapeutically treated mice with either 30 mg/kg or 60 mg/kg

402 BID or QD GS-621763 at 12 and 24 hrs (n=10 for all treatment groups, except n=8 for 60 mg/kg,

403 12 hr QD treatment group, and n=7 for vehicle group).

404 Data were analyzed using two-way ANOVA (weight loss and lung function) and Kruskal-Wallis

405 test (lung titer, lung viral RNA, and pathology scores), *$p<0.05$, **$p<0.005$, ***$p<0.0005$,

406 ****$p<0.0001$.

407

408 **Figure 4. Evaluation of therapeutic intervention of GS-621763 in comparison to**

409 **molnupiravir (MPV).**

410 (A) Depicted is the % starting weight in therapeutically treated mice with either 30 mg/kg or 60

411 mg/kg GS-621763 or MPV at 12 or 24 hrs (n=10 for all treatment groups). All mice were

412 infected with $1x10^4$ PFU SARS-CoV-2 MA10.

413 (B) Lung viral titers in therapeutically treated mice with either 30 mg/kg or 60 mg/kg GS-

414 621763 or MPV at 12 or 24 hrs (n=10 for all treatment groups). All mice were infected with

415 $1x10^4$ PFU SARS-CoV-2 MA10. Limit of detection (LoD).

416 (C) Viral N RNA in therapeutically treated mice with either 30 mg/kg or 60 mg/kg GS-621763

417 or MPV at 12 or 24 hrs (n=10 for all treatment groups). All mice were infected with $1x10^4$ PFU

418 SARS-CoV-2 MA10.

419 (D) Pulmonary function in therapeutically treated mice with either 30 mg/kg or 60mg/kg GS-

420 621763 or MPV at 12 or 24 hrs (n=4 for all treatment groups). All mice were infected with $1x10^4$

421 PFU SARS-CoV-2 MA10.

422 (F and G) Lung pathology in the therapeutically treated mice with either 30 mg/kg or 60 mg/kg
423 GS-621763 or MPV at 12or 24 hrs (n=10 for all treatment groups). All mice were infected with
424 $1x10^4$ PFU SARS-CoV-2 MA10.
425 Data were analyzed using two-way ANOVA (weight loss and lung function) and Kruskal-Wallis
426 test (lung titer, lung viral RNA, and pathology scores), *p<0.05, **p<0.005, ***p<0.0005,
427 ****p<0.0001
428
429 **Supplemental Figure 1. In vitro potency and toxicity of GS-621763, RDV, and GS-441524**
430 **in A549-hACE2 cells**
431 (A) Raw data for the inhibition of SARS-CoV-2 replication by GS-621763, RDV, and GS-
432 441521 in A459-hACE2 cells measured through quantitation of SARS-CoV-2 expressed nano
433 luciferase (nLuc), measured in triplicates.
434 (B) Raw data for cytotoxicity in A459-hACE2 cells treated with GS-621763, RDV, and GS-
435 441521 in A459-hACE2 cells measured via CellTiter-Glo, (measured in triplicates).
436 C) Raw data for the inhibition of SARS-CoV-2-Fluc replication by GS-621763, RDV, and GS-
437 441521 in NHBE cultures measured through quantitation of SARS-CoV-2 expressed firefly
438 luciferase (Fluc), measured in duplicates, repeated twice.
439
440 **Supplemental Figure 2. Molnupiravir mouse plasma pharmacokinetics**
441 Plasma Pharmacokinetics of N-hydroxycytidine (NHC) in uninfected Balb/c mice following
442 daily oral administration of molnupiravir at either 60 or 200 mg/kg (as either 30 or 100
443 mg/kg/dose given BID; molnupiravir at all timepoints).
444

445 **Material and Methods**

446 **Small molecule drug synthesis and formulation**

447 GS-621763, RDV, and GS-441524 were synthesized at Gilead Sciences Inc., and their chemical
448 identity and purity were determined by nuclear magnetic resonance, and high-performance
449 liquid chromatography (HPLC) analysis (*27*). Molnupiravir was purchased from
450 MedChemExpress LLC (NJ, USA) with a purity of 95% based on HPLC analysis.

451 Small molecules were solubilized in 100% DMSO for in vitro studies and in vehicle
452 containing 2.5% DMSO; 10% Kolliphor HS-15; 10% Labrasol; 2.5% Propylene glycol; 75%
453 Water (final formulation pH 2) (for GS-621763) and in vehicle containing 2.5% Kolliphor RH-
454 40, 10% Polyethylene glycol 300, 87.5% Water (for MPV) for in vivo studies. GS-621763, GS-
455 441524, GS-5734 were made available to the University of North Carolina (UNC) at Chapel Hill
456 under a materials transfer agreement with Gilead Sciences.

457

458 **In vivo plasma pharmacokinetic analysis of GS-621763 and molnupiravir (MPV)**

459 Mice were orally administered either a single dose of GS-621763 (in vehicle containing
460 2.5% DMSO; 10% Kolliphor HS-15; 10% Labrasol; 2.5% Propylene glycol; 75% Water (final
461 formulation pH 2) or two doses of molnupiravir (in vehicle containing 2.5% Kolliphor RH-40,
462 10% Polyethylene glycol 300, 87.5% Water) (BID, 12 hours apart). GS-621763 was given at
463 either 5 or 20 mg/kg and MPV at either 30 or 100 mg/kg. Plasma was serially isolated from 4
464 mice at 0.25, 1, 2, 8 and 24 hrs post GS-621763 administration. Plasma was isolated from
465 alternating groups of 4 mice per timepoint at 0.5, 2, 6, 12 (pre-second dose), 12.5, 18 and 24
466 hrs post MPV administration. 20 µl of plasma was added to a mixture containing 250 µl of
467 methanol and 25 µL of internal standard solution and centrifuged. 250 µl of resulting

468 supernatant was then transferred, filtered (Agilent Captiva 96, 0.2 µm) and dried under a stream
469 of nitrogen at 40 ºC. Following reconstitution in a mixture of 5% acetonitrile and 95% water, a
470 10 µl aliquot was injected onto an LC-MS/MS system. Plasma concentrations of either GS-
471 621763 and GS-441524 or MPV and N-hydroxycytidine (NHC) were determined using 8 to 10-
472 point calibration curves spanning at least 3 orders of magnitude with quality control samples to
473 ensure accuracy and precision, prepared in normal mouse plasma. Analytes were separated by a
474 50 mm × 3.0 mm, 2.55 µm Synergi Polar-RP column (Phenomenex) using a multi-stage linear
475 gradient from 5% to 95% acetonitrile in mobile phase A at a flow rate of 1 ml/min.
476

477 **Quantitation of GS-441524 metabolites in the lung following oral GS-621763**
478 **administration in *Balb/c* mice**

479 Lungs from all mice administered GS-621763 were quickly isolated at 24 hrs post-dose
480 and immediately snap frozen in liquid nitrogen. On dry ice, frozen lung samples were
481 pulverized and weighed. Dry ice-cold extraction buffer containing 0.1% potassium hydroxide
482 and 67 mM ethylenediamine tetraacetic acid (EDTA) in 70% methanol, containing 0.5µM
483 chloro-adenosine triphosphate as internal standard was added and homogenized. After
484 centrifugation at 20,000 × g for 20 minutes, supernatants were transferred and dried in a
485 centrifuging evaporator. Dried samples were then reconstituted with 60 µL of mobile phase A,
486 containing 3 mM ammonium formate (pH 5) with 10 mM dimethylhexylamine (DMH) in
487 water, centrifuged at 20,000 × g for 20 minutes and final supernatants transferred to HPLC
488 injection vials. An aliquot of 10 µl was subsequently injected onto an API 6500 LC/MS/MS
489 system for analysis of GS-441524 and its phosphorylated metabolites, performed using a
490 similar method as described previously (*18*).

491

492 **Viruses and plaque assay**

493 Recombinant SARS-CoV-2 MA10 virus was generated as described previously (*30*). For
494 virus titration by plaque assay, the caudal lobe of the right lung was homogenized in PBS, and
495 the resulting homogenate was serial-diluted and inoculated onto confluent monolayers of Vero
496 E6 cells, followed by agarose overlay. Plaques were visualized with overlay of neutral red dye
497 on day 3 after infection (*30*).

498

499 **In vitro assays for antiviral activity**

500 A549-hACE2 cells were plated at a density of 20,000 cells/well/100 µl in black-walled
501 clear-bottom 96-well plates 24 hrs prior to infection. Compounds GS-621763, GS-5734, GS-
502 441524, were diluted in 100% DMSO (1:3) resulting in a 1000X dose response from 10 to 0.002
503 mM (10 to 0.002 µM final). All conditions were performed in triplicate. At BSL3, medium was
504 removed, and cells were infected with 100 µl SARS-CoV-2 nLUC (MOI 0.008) for 1 h at 37 ˚C
505 after which virus was removed, wells were washed (150 µl) with infection media (DMEM, 4%
506 FBS, 1X antibiotic/antimycotic) and infection media (100 µl) containing a dose response of drug
507 was added. Plates were incubated at 37 ˚C for 48 hrs. NanoGlo assay was performed 48 hpi.
508 Sister plates were exposed to drug but not infected to gauge cytotoxicity via CellTiter-Glo assay
509 (CTG, Promega, Madison, WI), 48 hrs post treatment.

510 Normal human bronchial epithelial (NHBE) cells (donor 41219) were purchased from
511 Lonza (Walkersville, MD Cat# CC-2540) and maintained in Bronchial Epithelial Cell Growth
512 Medium (BEGM) (Lonza, Walkersville, MD, Cat# CC-3170) with all provided supplements in
513 the BulletKit. Cells are passaged 2-3 times per week to maintain sub-confluent densities and are

514 used for experiments at passages 2-4. NHBE cells were seeded in 24-well plates at $1x10^5$ cells in
515 a final volume of 0.5 ml BEGM™ Bronchial Epithelial Cell Growth Medium (BulletKit™;
516 Lonza, Basel, SW). Cultures were incubated overnight 37 °C with 5% CO_2. On the following
517 day, media was replaced with 0.5 ml growth medium. Cultures were treated with 1:3 serial
518 dilutions of compound using the HP D300e digital dispenser with normalization to the highest
519 concentration of DMSO in all wells (<1% final volume). The cells were then infected with 0.1
520 ml SARS-CoV-2-Fluc diluted in BEGM media at MOI = 5. Uninfected and untreated wells were
521 included as controls to determine compound efficacy against SARS-CoV-2-Fluc. Following
522 incubation with compound and virus for 24 hrs at 37 °C with 5% CO_2, culture supernatant was
523 removed from each well and replaced with 0.3 ml of ONE-Glo luciferase reagent (Promega,
524 Madison, WI). The plates were shaken at 400 rpm for 10 min at room temperature. 0.2 ml of
525 supernatant from each well was transferred to a 96-well opaque plate (Corning) and
526 luminescence signal was measured using an EnVision plate reader (PerkinElmer). Values were
527 normalized to the uninfected and infected DMSO controls (0% and 100% infection,
528 respectively). Data was fit using a four-parameter non-linear regression analysis using Graphpad
529 Prism. EC_{50} values were then determined as the concentration reducing the firefly luciferase
530 signal by 50%. The compiled data was generated based on least two independent experimental
531 replicates, each containing four technical replicates for each concentration.

532 **Mouse studies and in vivo infections**

533 All mouse studies were performed at the University of North Carolina (Animal Welfare
534 Assurance #A3410-01) using protocols (#20-059) approved by the University of North Carolina
535 Institutional Animal Care and Use Committee. All animal work was approved by the
536 Institutional Animal Care and Use Committee at University of North Carolina at Chapel Hill

537 according to guidelines outlined by the Association for the Assessment and Accreditation of
538 Laboratory Animal Care and the US Department of Agriculture. All work was performed with
539 approved standard operating procedures and safety conditions for SARS-CoV-2. Our
540 institutional BSL3 facilities are designed to conform to the safety requirements recommended by
541 Biosafety in Microbiological and Biomedical Laboratories, the US Department of Health and
542 Human Services, the Public Health Service, the Centers for Disease Control and Prevention, and
543 the National Institutes of Health. Laboratory safety plans have been submitted, and the facility
544 has been approved for use by the University of North Carolina Department of Environmental
545 Health and Safety and the Centers for Disease Control and Prevention.

546 Even groups (n=10, or less as indicated) of 10-week-old female BALB/c mice (Envigo;
547 #047) were used in all in vivo efficacy studies. For infection, mice were anesthetized with a
548 mixture of ketamine/xylazine and infected with 10^4 PFU of SARS-CoV-2 MA10 in 50 µl PBS
549 intranasally. Vehicle or GS-621673 was administered orally at the dosages and timepoints as
550 indicated. Mice were monitored daily for body weight changes and for lung function by whole-
551 body plethysmography. At 4 dpi, mice were euthanized, and lung tissue was harvested for viral
552 titer analysis, RNA and histology, and lung congestion scores were estimated (*30*). Samples for
553 viral load determination and for RNA isolation were stored at −80 °C until used; histology
554 samples were inactivated in 10% NBF and stored at 4 °C until further processing.

555

556 **Histology and lung pathology scoring**

557 Two separate lung pathology scoring scales, Matute-Bello and Diffuse Alveolar Damage
558 (DAD), were used to quantify acute lung injury (ALI) (*19*).

559 For Matute-Bello scoring samples were blinded and three random fields of lung tissue
560 were chosen and scored for the following: (A) neutrophils in alveolar space (none = 0, 1–5 cells =

561 1, > 5 cells = 2), (B) neutrophils in interstitial space (none = 0, 1–5 cells = 1, > 5 cells = 2), (C)
562 hyaline membranes (none = 0, one membrane = 1, > 1 membrane = 2), (D) Proteinaceous debris
563 in air spaces (none = 0, one instance = 1, > 1 instance = 2), (E) alveolar septal thickening (< 2Å~
564 mock thickness = 0, 2–4Å~ mock thickness = 1, > 4Å~ mock thickness = 2). Scores from A–E
565 were put into the following formula score = [(20x A) + (14 x B) + (7 x C) + (7 x D) + (2 x E)]/100
566 to obtain a lung injury score per field and then averaged for the final score for that sample.
567 In a similar way, for DAD scoring, three random fields of lung tissue were scored for the
568 in a blinded manner for: 1= absence of cellular sloughing and necrosis, 2= uncommon solitary cell
569 sloughing and necrosis (1–2 foci/field), 3=multifocal (3+foci) cellular sloughing and necrosis with
570 uncommon septal wall hyalinization, or 4=multifocal (>75% of field) cellular sloughing and
571 necrosis with common and/or prominent hyaline membranes. To obtain the final DAD score per
572 mouse, the scores for the three fields per mouse were averaged.

573 **RNA isolation and RT-qPCR**

574 Mouse tissue from SARS-CoV-2 infected mice was homogenized using glass beads in
575 TRIzol Reagent (Invitrogen). Equal volume of 100% EtOH was mixed with the TRIzol
576 homogenate and processed using Direct-Zol RNA MiniPrep Kit (Zymo) to extract viral RNA.
577 Optional DNase I treatment was conducted to ensure the adequate removal of unwanted DNA.
578 Eluted RNA was coupled with TaqMan Fast Virus 1-step Master Mix (Applied Biosystems) and
579 nCOV_N1 primers/probe (IDT) to quantify viral load via reverse transcription – quantitative
580 polymerase chain reaction (RT-qPCR). Samples were plated on a MicroAmp EnduraPlate
581 (Applied Biosystems) and run using a QuantStudio 6 Real-Time PCR System (Applied
582 Biosystems) to obtain viral titers. The following PCR program was run: 50 °C for 5 minutes, 95

583 °C for 20 seconds, followed by 45 cycles of 95 °C for 3 seconds and 60°C for 30 seconds. The
584 sequences of the 2019-nCOV_N1 primers and probe were as follows: Forward primer: GAC
585 CCC AAA ATC AGC GAA AT, Reverse primer: TCT GGT TAC TGC CAG TTG AAT CTG,
586 Probe: AC CCC GCA TT ACG TTT GGT GGA CC (CDC N1 qRT-PCR assay (*42*). SARS-
587 CoV-2 standard curve RNA was produced by PCR amplification of SARS-CoV-2 nucleocapsid
588 by which a 5' T7 polymerase promoter was introduced. This amplicon was used as template to
589 generate in vitro transcribed RNA which was then quantified and serially diluted (108 – 101
590 copies/µl).

591 **Acknowledgement**

592 D.R.M. is funded by a Burroughs Wellcome Fund Postdoctoral Enrichment Program Award and a Hanna
593 H. Gray Fellowship from the Howard Hughes Medical Institute and was supported by an NIH NIAID T32
594 AI007151 and an NIH F32 AI152296. This work was supported by NIAID R01 AI132178 and
595 R01AI132178-04S1 (T.P.S. and R.S.B.) and an NIH animal models contract (HHSN272201700036I) to
596 R.S.B. This project was supported in part by the North Carolina Policy Collaboratory at University of
597 North Carolina at Chapel Hill with funding from the North Carolina Coronavirus Relief Fund established
598 and appropriated by the North Carolina General Assembly.
599 Animal histopathology services were performed by the Animal Histopathology & Laboratory Medicine
600 Core at the University of North Carolina, which is supported in part by an NCI Center Core Support
601 Grant (5P30CA016086-41) to the UNC Lineberger Comprehensive Cancer Center.
602

603 **Competing interest**

604 These authors are employees of Gilead Sciences and hold stock in Gilead Sciences: Rao Kalla,
605 Kwon Chun, Venice Du Pont, Darius Babusis, Jennifer Tang, Eisuke Murakami, Raju

606 Subramanian, Kimberly T Barrett, Blake J. Bleier, Roy Bannister, Joy Y. Feng, John P. Bilello,
607 Tomas Cihlar, and Richard L. Mackman

608

609 **Literature**

610 1. P. Zhou, X. L. Yang, X. G. Wang, B. Hu, L. Zhang, W. Zhang, H. R. Si, Y. Zhu, B. Li,
611 C. L. Huang, H. D. Chen, J. Chen, Y. Luo, H. Guo, R. D. Jiang, M. Q. Liu, Y. Chen, X.
612 R. Shen, X. Wang, X. S. Zheng, K. Zhao, Q. J. Chen, F. Deng, L. L. Liu, B. Yan, F. X.
613 Zhan, Y. Y. Wang, G. F. Xiao, Z. L. Shi, A pneumonia outbreak associated with a new
614 coronavirus of probable bat origin. *Nature* **579**, 270-273 (2020).
615 2. N. Zhu, D. Zhang, W. Wang, X. Li, B. Yang, J. Song, X. Zhao, B. Huang, W. Shi, R. Lu,
616 P. Niu, F. Zhan, X. Ma, D. Wang, W. Xu, G. Wu, G. F. Gao, W. Tan, I. China Novel
617 Coronavirus, T. Research, A Novel Coronavirus from Patients with Pneumonia in China,
618 2019. *N Engl J Med* **382**, 727-733 (2020).
619 3. J. H. University. (2020).
620 4. A. Binagwaho, K. Mathewos, S. Davis, Time for the ethical management of COVID-19
621 vaccines. *Lancet Glob Health*, (2021).
622 5. E. Aryeetey, E. Engebretsen, A. Gornitzka, P. Maassen, S. Stolen, A step backwards in
623 the fight against global vaccine inequities. *Lancet* **397**, 23-24 (2021).
624 6. A. Asundi, C. O'Leary, N. Bhadelia, Global COVID-19 vaccine inequity: The scope, the
625 impact, and the challenges. *Cell Host Microbe* **29**, 1036-1039 (2021).
626 7. J. R. Barrett, S. Belij-Rammerstorfer, C. Dold, K. J. Ewer, P. M. Folegatti, C. Gilbride,
627 R. Halkerston, J. Hill, D. Jenkin, L. Stockdale, M. K. Verheul, P. K. Aley, B. Angus, D.
628 Bellamy, E. Berrie, S. Bibi, M. Bittaye, M. W. Carroll, B. Cavell, E. A. Clutterbuck, N.
629 Edwards, A. Flaxman, M. Fuskova, A. Gorringe, B. Hallis, S. Kerridge, A. M. Lawrie, A.
630 Linder, X. Liu, M. Madhavan, R. Makinson, J. Mellors, A. Minassian, M. Moore, Y.
631 Mujadidi, E. Plested, I. Poulton, M. N. Ramasamy, H. Robinson, C. S. Rollier, R. Song,
632 M. D. Snape, R. Tarrant, S. Taylor, K. M. Thomas, M. Voysey, M. E. E. Watson, D.
633 Wright, A. D. Douglas, C. M. Green, A. V. S. Hill, T. Lambe, S. Gilbert, A. J. Pollard, C.
634 V. T. G. Oxford, Phase 1/2 trial of SARS-CoV-2 vaccine ChAdOx1 nCoV-19 with a
635 booster dose induces multifunctional antibody responses. *Nat Med* **27**, 279-288 (2021).
636 8. J. Grein, N. Ohmagari, D. Shin, G. Diaz, E. Asperges, A. Castagna, T. Feldt, G. Green,
637 M. L. Green, F. X. Lescure, E. Nicastri, R. Oda, K. Yo, E. Quiros-Roldan, A.
638 Studemeister, J. Redinski, S. Ahmed, J. Bernett, D. Chelliah, D. Chen, S. Chihara, S. H.
639 Cohen, J. Cunningham, A. D'Arminio Monforte, S. Ismail, H. Kato, G. Lapadula, E.
640 L'Her, T. Maeno, S. Majumder, M. Massari, M. Mora-Rillo, Y. Mutoh, D. Nguyen, E.
641 Verweij, A. Zoufaly, A. O. Osinusi, A. DeZure, Y. Zhao, L. Zhong, A. Chokkalingam, E.
642 Elboudwarej, L. Telep, L. Timbs, I. Henne, S. Sellers, H. Cao, S. K. Tan, L.
643 Winterbourne, P. Desai, R. Mera, A. Gaggar, R. P. Myers, D. M. Brainard, R. Childs, T.
644 Flanigan, Compassionate Use of Remdesivir for Patients with Severe Covid-19. *N Engl J*
645 *Med* **382**, 2327-2336 (2020).

9. J. H. Beigel, K. M. Tomashek, L. E. Dodd, A. K. Mehta, B. S. Zingman, A. C. Kalil, E. Hohmann, H. Y. Chu, A. Luetkemeyer, S. Kline, D. Lopez de Castilla, R. W. Finberg, K. Dierberg, V. Tapson, L. Hsieh, T. F. Patterson, R. Paredes, D. A. Sweeney, W. R. Short, G. Touloumi, D. C. Lye, N. Ohmagari, M. D. Oh, G. M. Ruiz-Palacios, T. Benfield, G. Fatkenheuer, M. G. Kortepeter, R. L. Atmar, C. B. Creech, J. Lundgren, A. G. Babiker, S. Pett, J. D. Neaton, T. H. Burgess, T. Bonnett, M. Green, M. Makowski, A. Osinusi, S. Nayak, H. C. Lane, A.-S. G. Members, Remdesivir for the Treatment of Covid-19 - Final Report. *N Engl J Med* **383**, 1813-1826 (2020).

10. D. F. Robbiani, C. Gaebler, F. Muecksch, J. C. C. Lorenzi, Z. Wang, A. Cho, M. Agudelo, C. O. Barnes, A. Gazumyan, S. Finkin, T. Hagglof, T. Y. Oliveira, C. Viant, A. Hurley, H. H. Hoffmann, K. G. Millard, R. G. Kost, M. Cipolla, K. Gordon, F. Bianchini, S. T. Chen, V. Ramos, R. Patel, J. Dizon, I. Shimeliovich, P. Mendoza, H. Hartweger, L. Nogueira, M. Pack, J. Horowitz, F. Schmidt, Y. Weisblum, E. Michailidis, A. W. Ashbrook, E. Waltari, J. E. Pak, K. E. Huey-Tubman, N. Koranda, P. R. Hoffman, A. P. West, Jr., C. M. Rice, T. Hatziioannou, P. J. Bjorkman, P. D. Bieniasz, M. Caskey, M. C. Nussenzweig, Convergent antibody responses to SARS-CoV-2 in convalescent individuals. *Nature* **584**, 437-442 (2020).

11. S. J. Zost, P. Gilchuk, R. E. Chen, J. B. Case, J. X. Reidy, A. Trivette, R. S. Nargi, R. E. Sutton, N. Suryadevara, E. C. Chen, E. Binshtein, S. Shrihari, M. Ostrowski, H. Y. Chu, J. E. Didier, K. W. MacRenaris, T. Jones, S. Day, L. Myers, F. Eun-Hyung Lee, D. C. Nguyen, I. Sanz, D. R. Martinez, P. W. Rothlauf, L. M. Bloyet, S. P. J. Whelan, R. S. Baric, L. B. Thackray, M. S. Diamond, R. H. Carnahan, J. E. Crowe, Jr., Rapid isolation and profiling of a diverse panel of human monoclonal antibodies targeting the SARS-CoV-2 spike protein. *Nat Med* **26**, 1422-1427 (2020).

12. D. Pinto, Y. J. Park, M. Beltramello, A. C. Walls, M. A. Tortorici, S. Bianchi, S. Jaconi, K. Culap, F. Zatta, A. De Marco, A. Peter, B. Guarino, R. Spreafico, E. Cameroni, J. B. Case, R. E. Chen, C. Havenar-Daughton, G. Snell, A. Telenti, H. W. Virgin, A. Lanzavecchia, M. S. Diamond, K. Fink, D. Veesler, D. Corti, Cross-neutralization of SARS-CoV-2 by a human monoclonal SARS-CoV antibody. *Nature* **583**, 290-295 (2020).

13. A.-T. L.-C. S. Group, J. D. Lundgren, B. Grund, C. E. Barkauskas, T. L. Holland, R. L. Gottlieb, U. Sandkovsky, S. M. Brown, K. U. Knowlton, W. H. Self, D. C. Files, M. K. Jain, T. Benfield, M. E. Bowdish, B. G. Leshnower, J. V. Baker, J. U. Jensen, E. M. Gardner, A. A. Ginde, E. S. Harris, I. S. Johansen, N. Markowitz, M. A. Matthay, L. Ostergaard, C. C. Chang, V. J. Davey, A. Goodman, E. S. Higgs, D. D. Murray, T. A. Murray, R. Paredes, M. K. B. Parmar, A. N. Phillips, C. Reilly, S. Sharma, R. L. Dewar, M. Teitelbaum, D. Wentworth, H. Cao, P. Klekotka, A. G. Babiker, A. C. Gelijns, V. L. Kan, M. N. Polizzotto, B. T. Thompson, H. C. Lane, J. D. Neaton, A Neutralizing Monoclonal Antibody for Hospitalized Patients with Covid-19. *N Engl J Med* **384**, 905-914 (2021).

14. M. P. O'Brien, E. Forleo-Neto, B. J. Musser, F. Isa, K. C. Chan, N. Sarkar, K. J. Bar, R. V. Barnabas, D. H. Barouch, M. S. Cohen, C. B. Hurt, D. R. Burwen, M. A. Marovich, P. Hou, I. Heirman, J. D. Davis, K. C. Turner, D. Ramesh, A. Mahmood, A. T. Hooper, J. D. Hamilton, Y. Kim, L. A. Purcell, A. Baum, C. A. Kyratsous, J. Krainson, R. Perez-Perez, R. Mohseni, B. Kowal, A. T. DiCioccio, N. Stahl, L. Lipsich, N. Braunstein, G. Herman, G. D. Yancopoulos, D. M. Weinreich, T. Covid-19 Phase 3 Prevention Trial,

692 Subcutaneous REGEN-COV Antibody Combination to Prevent Covid-19. *N Engl J Med*,
693 (2021).
694 15. R. E. Chen, X. Zhang, J. B. Case, E. S. Winkler, Y. Liu, L. A. VanBlargan, J. Liu, J. M.
695 Errico, X. Xie, N. Suryadevara, P. Gilchuk, S. J. Zost, S. Tahan, L. Droit, J. S. Turner,
696 W. Kim, A. J. Schmitz, M. Thapa, D. Wang, A. C. M. Boon, R. M. Presti, J. A.
697 O'Halloran, A. H. J. Kim, P. Deepak, D. Pinto, D. H. Fremont, J. E. Crowe, Jr., D. Corti,
698 H. W. Virgin, A. H. Ellebedy, P. Y. Shi, M. S. Diamond, Resistance of SARS-CoV-2
699 variants to neutralization by monoclonal and serum-derived polyclonal antibodies. *Nat*
700 *Med* **27**, 717-726 (2021).
701 16. P. Wang, M. S. Nair, L. Liu, S. Iketani, Y. Luo, Y. Guo, M. Wang, J. Yu, B. Zhang, P. D.
702 Kwong, B. S. Graham, J. R. Mascola, J. Y. Chang, M. T. Yin, M. Sobieszczyk, C. A.
703 Kyratsous, L. Shapiro, Z. Sheng, Y. Huang, D. D. Ho, Antibody resistance of SARS-
704 CoV-2 variants B.1.351 and B.1.1.7. *Nature* **593**, 130-135 (2021).
705 17. D. R. Martinez, A. Schäfer, S. R. Leist, D. Li, K. Gully, B. Yount, J. Y. Feng, E. Bunyan,
706 D. P. Porter, T. Cihlar, S. A. Montgomery, B. F. Haynes, R. S. Baric, M. C.
707 Nussenzweig, T. P. Sheahan, Prevention and therapy of SARS-CoV-2 and the B.1.351
708 variant in mice. *Cell Rep* **36**, 109450 (2021).
709 18. T. P. Sheahan, A. C. Sims, R. L. Graham, V. D. Menachery, L. E. Gralinski, J. B. Case,
710 S. R. Leist, K. Pyrc, J. Y. Feng, I. Trantcheva, R. Bannister, Y. Park, D. Babusis, M. O.
711 Clarke, R. L. Mackman, J. E. Spahn, C. A. Palmiotti, D. Siegel, A. S. Ray, T. Cihlar, R.
712 Jordan, M. R. Denison, R. S. Baric, Broad-spectrum antiviral GS-5734 inhibits both
713 epidemic and zoonotic coronaviruses. *Sci Transl Med* **9**, (2017).
714 19. T. P. Sheahan, A. C. Sims, S. R. Leist, A. Schafer, J. Won, A. J. Brown, S. A.
715 Montgomery, A. Hogg, D. Babusis, M. O. Clarke, J. E. Spahn, L. Bauer, S. Sellers, D.
716 Porter, J. Y. Feng, T. Cihlar, R. Jordan, M. R. Denison, R. S. Baric, Comparative
717 therapeutic efficacy of remdesivir and combination lopinavir, ritonavir, and interferon
718 beta against MERS-CoV. *Nat Commun* **11**, 222 (2020).
719 20. T. P. Sheahan, A. C. Sims, S. Zhou, R. L. Graham, A. J. Pruijssers, M. L. Agostini, S. R.
720 Leist, A. Schafer, K. H. Dinnon, 3rd, L. J. Stevens, J. D. Chappell, X. Lu, T. M. Hughes,
721 A. S. George, C. S. Hill, S. A. Montgomery, A. J. Brown, G. R. Bluemling, M. G.
722 Natchus, M. Saindane, A. A. Kolykhalov, G. Painter, J. Harcourt, A. Tamin, N. J.
723 Thornburg, R. Swanstrom, M. R. Denison, R. S. Baric, An orally bioavailable broad-
724 spectrum antiviral inhibits SARS-CoV-2 in human airway epithelial cell cultures and
725 multiple coronaviruses in mice. *Sci Transl Med* **12**, (2020).
726 21. A. Wahl, L. E. Gralinski, C. E. Johnson, W. Yao, M. Kovarova, K. H. Dinnon, 3rd, H.
727 Liu, V. J. Madden, H. M. Krzystek, C. De, K. K. White, K. Gully, A. Schafer, T. Zaman,
728 S. R. Leist, P. O. Grant, G. R. Bluemling, A. A. Kolykhalov, M. G. Natchus, F. B. Askin,
729 G. Painter, E. P. Browne, C. D. Jones, R. J. Pickles, R. S. Baric, J. V. Garcia, SARS-
730 CoV-2 infection is effectively treated and prevented by EIDD-2801. *Nature* **591**, 451-457
731 (2021).
732 22. W. Fischer, J. J. Eron, W. Holman, M. S. Cohen, L. Fang, L. J. Szewczyk, T. P. Sheahan,
733 R. Baric, K. R. Mollan, C. R. Wolfe, E. R. Duke, M. M. Azizad, K. Borroto-Esoda, D. A.
734 Wohl, A. J. Loftis, P. Alabanza, F. Lipansky, W. P. Painter, Molnupiravir, an Oral
735 Antiviral Treatment for COVID-19. *medRxiv*, (2021).
736 23. B. N. Williamson, F. Feldmann, B. Schwarz, K. Meade-White, D. P. Porter, J. Schulz, N.
737 van Doremalen, I. Leighton, C. Kwe Yinda, L. Perez-Perez, A. Okumura, J. Lovaglio, P.

W. Hanley, G. Saturday, C. M. Bosio, S. Anzick, K. Barbian, T. Cihlar, C. Martens, D. P. Scott, V. J. Munster, E. de Wit, Clinical benefit of remdesivir in rhesus macaques infected with SARS-CoV-2. *bioRxiv*, (2020).

24. D. R. Owen, C. M. N. Allerton, A. S. Anderson, L. Aschenbrenner, M. Avery, S. Berritt, B. Boras, R. D. Cardin, A. Carlo, K. J. Coffman, A. Dantonio, L. Di, H. Eng, R. Ferre, K. S. Gajiwala, S. A. Gibson, S. E. Greasley, B. L. Hurst, E. P. Kadar, A. S. Kalgutkar, J. C. Lee, J. Lee, W. Liu, S. W. Mason, S. Noell, J. J. Novak, R. S. Obach, K. Ogilvie, N. C. Patel, M. Pettersson, D. K. Rai, M. R. Reese, M. F. Sammons, J. G. Sathish, R. S. P. Singh, C. M. Steppan, A. E. Stewart, J. B. Tuttle, L. Updyke, P. R. Verhoest, L. Wei, Q. Yang, Y. Zhu, An Oral SARS-CoV-2 M^{pro} Inhibitor Clinical Candidate for the Treatment of COVID-19. *medRxiv*, 2021.2007.2028.21261232 (2021).
25. S. S. Good, J. Westover, K. H. Jung, X. J. Zhou, A. Moussa, P. La Colla, G. Collu, B. Canard, J. P. Sommadossi, AT-527, a Double Prodrug of a Guanosine Nucleotide Analog, Is a Potent Inhibitor of SARS-CoV-2 In Vitro and a Promising Oral Antiviral for Treatment of COVID-19. *Antimicrob Agents Chemother* **65**, (2021).
26. A. J. Pruijssers, A. S. George, A. Schafer, S. R. Leist, L. E. Gralinksi, K. H. Dinnon, 3rd, B. L. Yount, M. L. Agostini, L. J. Stevens, J. D. Chappell, X. Lu, T. M. Hughes, K. Gully, D. R. Martinez, A. J. Brown, R. L. Graham, J. K. Perry, V. Du Pont, J. Pitts, B. Ma, D. Babusis, E. Murakami, J. Y. Feng, J. P. Bilello, D. P. Porter, T. Cihlar, R. S. Baric, M. R. Denison, T. P. Sheahan, Remdesivir Inhibits SARS-CoV-2 in Human Lung Cells and Chimeric SARS-CoV Expressing the SARS-CoV-2 RNA Polymerase in Mice. *Cell Rep* **32**, 107940 (2020).
27. R. L. Mackman, H. C. Hui, M. Perron, E. Murakami, C. Palmiotti, G. Lee, K. Stray, L. Zhang, B. Goyal, K. Chun, D. Byun, D. Siegel, S. Simonovich, V. Du Pont, J. Pitts, D. Babusis, A. Vijjapurapu, X. Lu, C. Kim, X. Zhao, J. Chan, B. Ma, D. Lye, A. Vandersteen, S. Wortman, K. T. Barrett, M. Toteva, R. Jordan, R. Subramanian, J. P. Bilello, T. Cihlar, Prodrugs of a 1'-CN-4-Aza-7,9-dideazaadenosine C-Nucleoside Leading to the Discovery of Remdesivir (GS-5734) as a Potent Inhibitor of Respiratory Syncytial Virus with Efficacy in the African Green Monkey Model of RSV. *J Med Chem* **64**, 5001-5017 (2021).
28. Y. J. Hou, K. Okuda, C. E. Edwards, D. R. Martinez, T. Asakura, K. H. Dinnon, 3rd, T. Kato, R. E. Lee, B. L. Yount, T. M. Mascenik, G. Chen, K. N. Olivier, A. Ghio, L. V. Tse, S. R. Leist, L. E. Gralinski, A. Schafer, H. Dang, R. Gilmore, S. Nakano, L. Sun, M. L. Fulcher, A. Livraghi-Butrico, N. I. Nicely, M. Cameron, C. Cameron, D. J. Kelvin, A. de Silva, D. M. Margolis, A. Markmann, L. Bartelt, R. Zumwalt, F. J. Martinez, S. P. Salvatore, A. Borczuk, P. R. Tata, V. Sontake, A. Kimple, I. Jaspers, W. K. O'Neal, S. H. Randell, R. C. Boucher, R. S. Baric, SARS-CoV-2 Reverse Genetics Reveals a Variable Infection Gradient in the Respiratory Tract. *Cell* **182**, 429-446 e414 (2020).
29. X. Xie, A. E. Muruato, X. Zhang, K. G. Lokugamage, C. R. Fontes-Garfias, J. Zou, J. Liu, P. Ren, M. Balakrishnan, T. Cihlar, C. K. Tseng, S. Makino, V. D. Menachery, J. P. Bilello, P. Y. Shi, A nanoluciferase SARS-CoV-2 for rapid neutralization testing and screening of anti-infective drugs for COVID-19. *Nat Commun* **11**, 5214 (2020).
30. S. R. Leist, K. H. Dinnon, 3rd, A. Schäfer, L. V. Tse, K. Okuda, Y. J. Hou, A. West, C. E. Edwards, W. Sanders, E. J. Fritch, K. L. Gully, T. Scobey, A. J. Brown, T. P. Sheahan, N. J. Moorman, R. C. Boucher, L. E. Gralinski, S. A. Montgomery, R. S. Baric, A

783 Mouse-Adapted SARS-CoV-2 Induces Acute Lung Injury and Mortality in Standard
784 Laboratory Mice. *Cell* **183**, 1070-1085.e1012 (2020).
785 31. R. L. Graham, E. F. Donaldson, R. S. Baric, A decade after SARS: strategies for
786 controlling emerging coronaviruses. *Nat Rev Microbiol* **11**, 836-848 (2013).
787 32. L. Rosenbaum, Escaping Catch-22 - Overcoming Covid Vaccine Hesitancy. *N Engl J*
788 *Med* **384**, 1367-1371 (2021).
789 33. B. Adhikari, P. Y. Cheah, Vaccine hesitancy in the COVID-19 era. *Lancet Infect Dis*,
790 (2021).
791 34. Z. Wang, F. Schmidt, Y. Weisblum, F. Muecksch, C. O. Barnes, S. Finkin, D. Schaefer-
792 Babajew, M. Cipolla, C. Gaebler, J. A. Lieberman, T. Y. Oliveira, Z. Yang, M. E.
793 Abernathy, K. E. Huey-Tubman, A. Hurley, M. Turroja, K. A. West, K. Gordon, K. G.
794 Millard, V. Ramos, J. Da Silva, J. Xu, R. A. Colbert, R. Patel, J. Dizon, C. Unson-
795 O'Brien, I. Shimeliovich, A. Gazumyan, M. Caskey, P. J. Bjorkman, R. Casellas, T.
796 Hatziioannou, P. D. Bieniasz, M. C. Nussenzweig, mRNA vaccine-elicited antibodies to
797 SARS-CoV-2 and circulating variants. *Nature* **592**, 616-622 (2021).
798 35. A. J. Brown, J. J. Won, R. L. Graham, K. H. Dinnon, 3rd, A. C. Sims, J. Y. Feng, T.
799 Cihlar, M. R. Denison, R. S. Baric, T. P. Sheahan, Broad spectrum antiviral remdesivir
800 inhibits human endemic and zoonotic deltacoronaviruses with a highly divergent RNA
801 dependent RNA polymerase. *Antiviral Res* **169**, 104541 (2019).
802 36. W. T. Harvey, A. M. Carabelli, B. Jackson, R. K. Gupta, E. C. Thomson, E. M. Harrison,
803 C. Ludden, R. Reeve, A. Rambaut, C.-G. U. Consortium, S. J. Peacock, D. L. Robertson,
804 SARS-CoV-2 variants, spike mutations and immune escape. *Nat Rev Microbiol* **19**, 409-
805 424 (2021).
806 37. D. C. Montefiori, P. Acharya, SnapShot: SARS-CoV-2 antibodies. *Cell Host Microbe* **29**,
807 1162-1162 e1161 (2021).
808 38. R. Martin, J. Li, A. Parvangada, J. Perry, T. Cihlar, H. Mo, D. Porter, E. Svarovskaia,
809 Genetic conservation of SARS-CoV-2 RNA replication complex in globally circulating
810 isolates and recently emerged variants from humans and minks suggests minimal pre-
811 existing resistance to remdesivir. *Antiviral Res* **188**, 105033 (2021).
812 39. Y. Liu, L. M. Yan, L. Wan, T. X. Xiang, A. Le, J. M. Liu, M. Peiris, L. L. M. Poon, W.
813 Zhang, Viral dynamics in mild and severe cases of COVID-19. *Lancet Infect Dis* **20**, 656-
814 657 (2020).
815 40. S. Zheng, J. Fan, F. Yu, B. Feng, B. Lou, Q. Zou, G. Xie, S. Lin, R. Wang, X. Yang, W.
816 Chen, Q. Wang, D. Zhang, Y. Liu, R. Gong, Z. Ma, S. Lu, Y. Xiao, Y. Gu, J. Zhang, H.
817 Yao, K. Xu, X. Lu, G. Wei, J. Zhou, Q. Fang, H. Cai, Y. Qiu, J. Sheng, Y. Chen, T.
818 Liang, Viral load dynamics and disease severity in patients infected with SARS-CoV-2 in
819 Zhejiang province, China, January-March 2020: retrospective cohort study. *BMJ* **369**,
820 m1443 (2020).
821 41. F. Zhou, T. Yu, R. Du, G. Fan, Y. Liu, Z. Liu, J. Xiang, Y. Wang, B. Song, X. Gu, L.
822 Guan, Y. Wei, H. Li, X. Wu, J. Xu, S. Tu, Y. Zhang, H. Chen, B. Cao, Clinical course
823 and risk factors for mortality of adult inpatients with COVID-19 in Wuhan, China: a
824 retrospective cohort study. *Lancet* **395**, 1054-1062 (2020).
825 42. X. Lu, L. Wang, S. K. Sakthivel, B. Whitaker, J. Murray, S. Kamili, B. Lynch, L.
826 Malapati, S. A. Burke, J. Harcourt, A. Tamin, N. J. Thornburg, J. M. Villanueva, S.
827 Lindstrom, US CDC Real-Time Reverse Transcription PCR Panel for Detection of
828 Severe Acute Respiratory Syndrome Coronavirus 2. *Emerg Infect Dis* **26**, (2020).

829

Figure 1

A

GS-441524

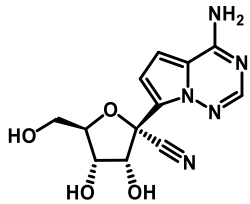

B

RDV

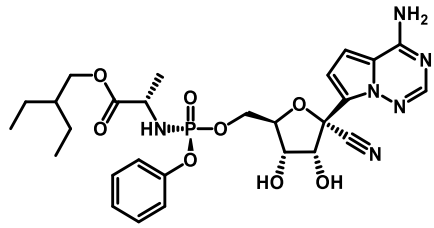

C

GS-621763

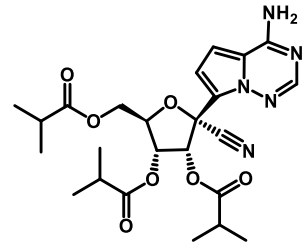

D

A549-hACE2

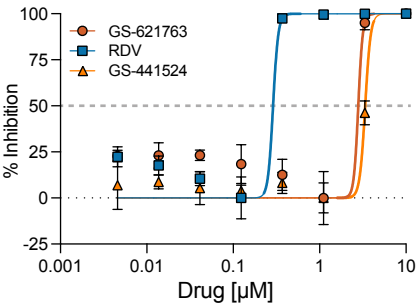

E

A549-hACE2

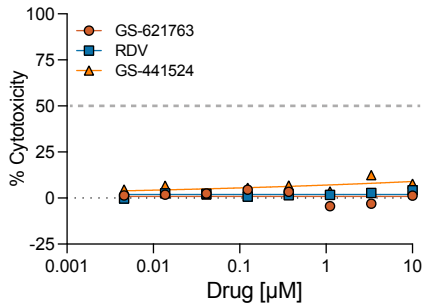

F

Antiviral Assay in Primary HAE

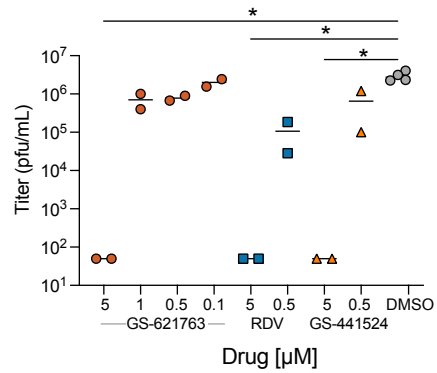

G

Normal Human Brochial Epithelial cells

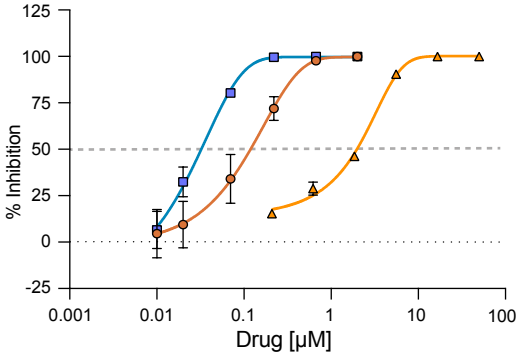

H

In vitro potency in human airway cells

Compound	Average EC_{50}(nM)	
	A549-hACE2	NHBE
GS-621763	2801	125 ± 22
RDV	293.8	37.1 ± 0.4
GS-441524	3368	2454 ± 63

Figure 4

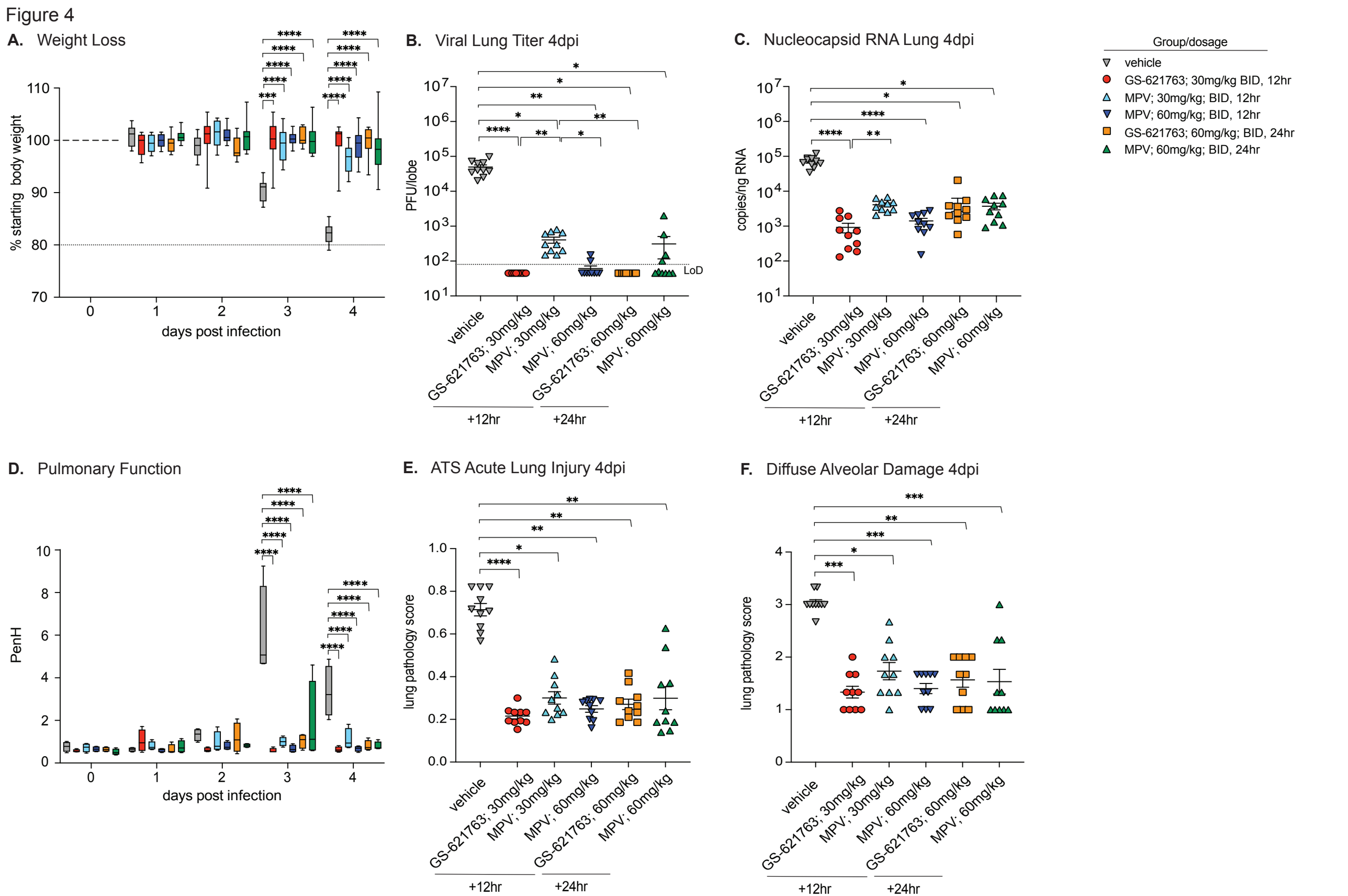
A. Weight Loss
% starting body weight
days post infection
B. Viral Lung Titer 4dpi
PFU/lobe
LoD
C. Nucleocapsid RNA Lung 4dpi
copies/ng RNA
Group/dosage
vehicle
GS-621763; 30mg/kg BID, 12hr
MPV; 30mg/kg; BID, 12hr
MPV; 60mg/kg; BID, 12hr
GS-621763; 60mg/kg; BID, 24hr
MPV; 60mg/kg; BID, 24hr
vehicle
GS-621763; 30mg/kg
MPV; 30mg/kg
MPV; 60mg/kg
GS-621763; 60mg/kg
MPV; 60mg/kg
+12hr
+24hr
D. Pulmonary Function
PenH
days post infection
E. ATS Acute Lung Injury 4dpi
lung pathology score
F. Diffuse Alveolar Damage 4dpi
lung pathology score

Figure 3

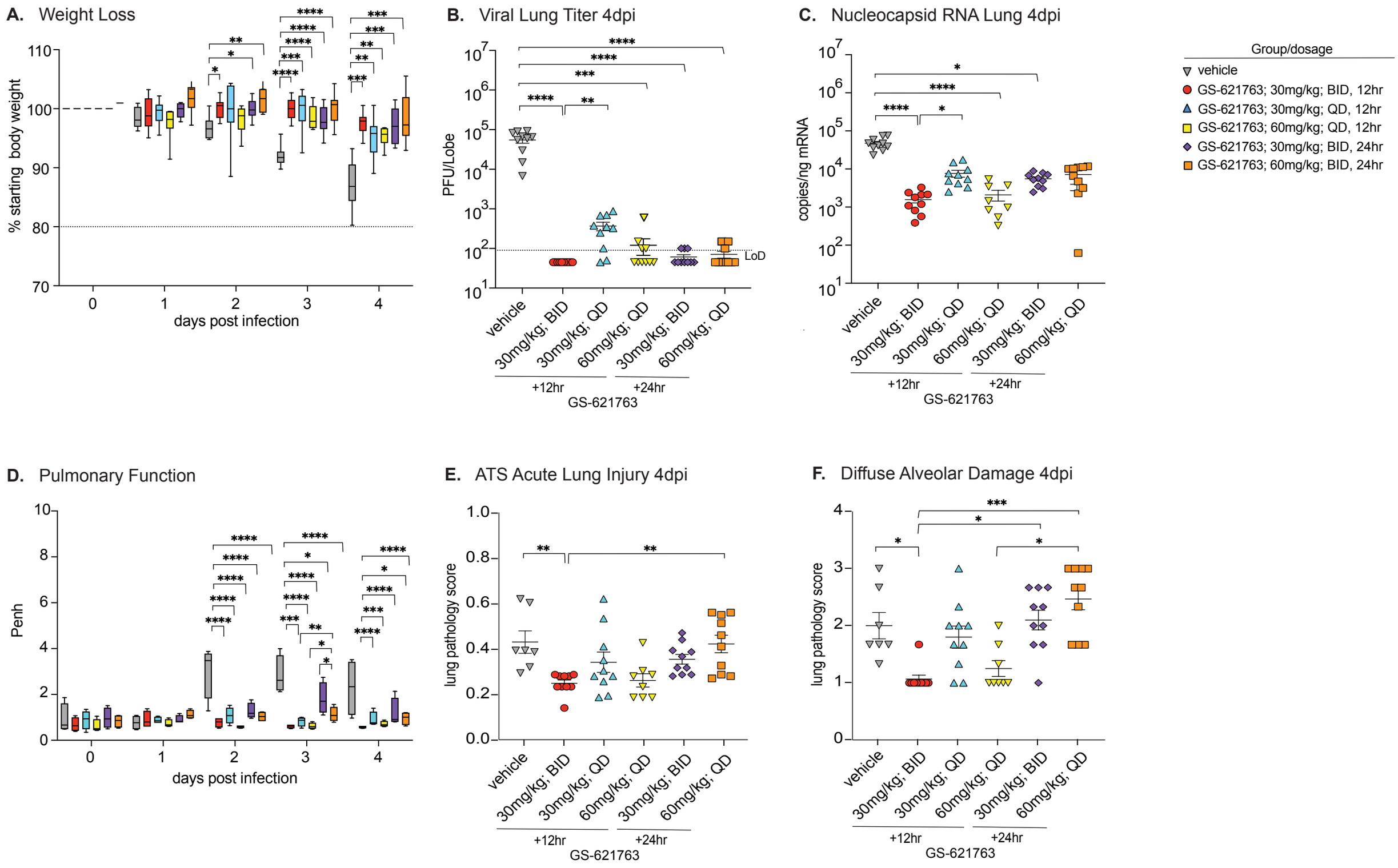
A. Weight Loss
% starting body weight
days post infection
B. Viral Lung Titer 4dpi
PFU/Lobe
LoD
C. Nucleocapsid RNA Lung 4dpi
copies/ng mRNA
vehicle
30mg/kg; BID
30mg/kg; QD
60mg/kg; QD
30mg/kg; BID
60mg/kg; QD
+12hr
+24hr
GS-621763
Group/dosage
vehicle
GS-621763; 30mg/kg; BID, 12hr
GS-621763; 30mg/kg; QD, 12hr
GS-621763; 60mg/kg; QD, 12hr
GS-621763; 30mg/kg; BID, 24hr
GS-621763; 60mg/kg; BID, 24hr
D. Pulmonary Function
Penh
days post infection
E. ATS Acute Lung Injury 4dpi
lung pathology score
F. Diffuse Alveolar Damage 4dpi
lung pathology score

Figure 2

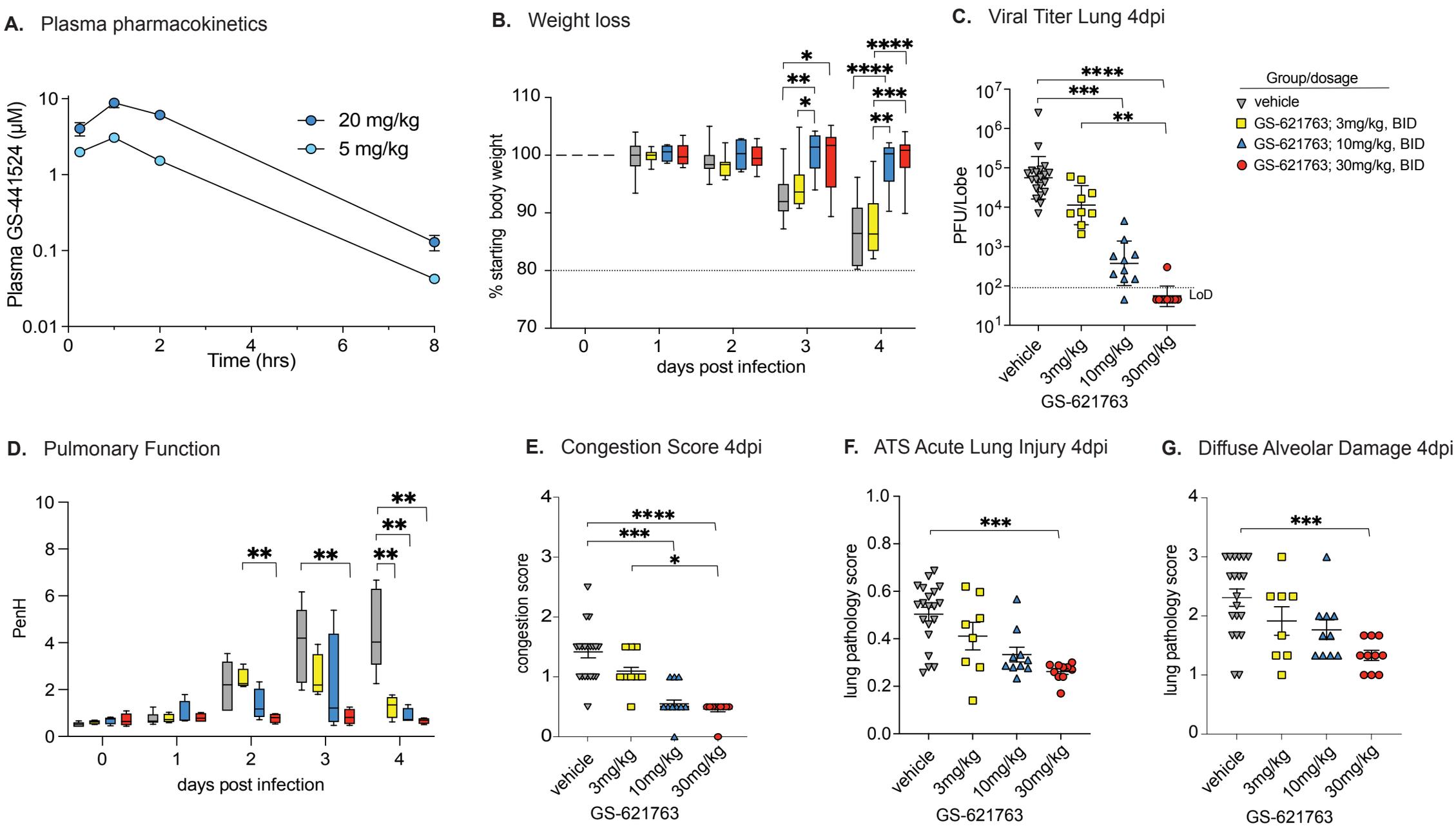
A. Plasma pharmacokinetics
Plasma GS-441524 (µM)
Time (hrs)
20 mg/kg
5 mg/kg
B. Weight loss
% starting body weight
days post infection
C. Viral Titer Lung 4dpi
PFU/Lobe
LoD
GS-621763
Group/dosage
vehicle
GS-621763; 3mg/kg, BID
GS-621763; 10mg/kg, BID
GS-621763; 30mg/kg, BID
D. Pulmonary Function
PenH
days post infection
E. Congestion Score 4dpi
congestion score
F. ATS Acute Lung Injury 4dpi
lung pathology score
G. Diffuse Alveolar Damage 4dpi
lung pathology score
vehicle
3mg/kg
10mg/kg
30mg/kg
GS-621763